Journal of Computational Dynamics
Vol. 14, 2026, pp. 36-52 (March 3, 2026)
doi:10.3934/jcd.2026005

CONVERGENCE OF ZEITLIN TRUNCATION FOR MULTILAYER CRITICAL LATITUDE PREDICTIONS OF QUASI-GEOSTROPHIC FLOW ON AN EARTH-LIKE PLANET

Arnout Franken[1], Sagy Ephrati[2],
Erwin Luesink[3] and Bernard Geurts[*1,4,5]

[1]Mathematics of Multiscale Modeling and Simulation, Faculty EEMCS,
University of Twente, P.O. Box 217, 7500 AE Enschede, The Netherlands

[2]Department of Mathematical Sciences,
Chalmers University of Technology & University of Gothenburg,
Göteborg, SE-412 96, Sweden

[3]Mathematics, Universiteit van Amsterdam, Amsterdam, The Netherlands

[4]Multiscale Physics, Faculty Technical Physics,
Eindhoven University of Technology,
P.O. Box 513, 5600 MB Eindhoven, The Netherlands

[5]Scientific Computing Group, Centrum voor Wiskunde en Informatica (CWI),
Science Park 123, 1098 XG Amsterdam, The Netherlands

Abstract. Long-term predictions of large-scale flow features on an Earth-like planet are crucial for developing global atmospheric model systems. Such predictions require computational models, i.e., governing PDE systems combined with appropriate numerical methods, to preserve essential structures of the underlying physical model over extended simulation periods. We present a Lie–Poisson formulation of the multi-layer quasi-geostrophhic (QG) equations on the full globe, mimicking the dynamics in the troposphere extended over the first 10 km of the atmosphere. The chosen computational modeling ensures consistency with the underlying structure and enables long-term simulations without the need for additional regularization, forcing, or numerical dissipation. Recent advancements in Lie–Poisson discretization that preserve energy, enstrophy, and higher-order moments of potential vorticity are extended to stratified QG multilayer systems on the sphere. We adopt Zeitlin discretization, which yields a finite-dimensional dynamical system conserving all numerically resolved Casimirs with machine-precision. Particular attention is given to the convergence of critical latitude (ϕ_{cl}) predictions upon increasing the spatial resolution per layer (N) and the number of layers in the model (M). A systematic parameter study quantifies (i) that the dependency of ϕ_{cl} on the resolution per layer N scales quadratically, showing near grid-independency for $N \geq 96$, and (ii) the critical latitude decreases with the number of layers M for modest radial resolutions of $M \leq 32$.

1. **Introduction.** The dynamics governing both the atmosphere and the oceans are fundamental to shaping Earth's weather systems and long-term climate patterns. In particular, large-scale circulation is strongly influenced by wave phenomena, such as Rossby and gravity waves. These wave-driven processes are highly sensitive to

latitude. A critical concept in this context is the so-called critical latitude ϕ_{cl}, defined as the latitude where the mean zonal flow speed coincides with the phase speed of the relevant wave [27]. Accurately predicting this latitude is essential for qualitative understanding as well as quantitative modeling of global circulation patterns in both atmospheric and oceanic contexts. Dynamics above and below the critical latitude play a pivotal role in phenomena such as wave breaking, shifts in jet stream position, and major climate oscillations, making it central to fields like meteorology, climate modeling, and geophysical fluid dynamics [38]. Notably, near the critical latitude, planetary Rossby waves may become unstable and break, triggering significant effects such as potential vorticity mixing, changes in the jet stream, and abrupt stratospheric warming events in polar regions [34]. The prevailing dynamical regimes differ substantially between equatorial zones and latitudes significantly higher than the critical latitude. Properly representing this holds promise for improving extended-range forecasts and deepening our understanding of wave–mean flow interactions [14].

Recently, we introduced a quasi-geostrophic (QG) model for flows on a rotating sphere that remains accurate across all latitudes away from the equator [19, 10]. This formulation employs Zeitlin's truncation strategy together with Lie–Poisson integration techniques [21, 19, 18, 8], preserving the structure of the governing equations. This framework has since been generalized to multi-layer configurations [11], enabling a more complete representation of the evolution of potential vorticity on the spherical domain across a wide range of scales. We confirmed the feasibility of these approaches through numerical experiments. In the current work, we utilize this multi-layer QG model to explore the prediction of the critical latitude ϕ_{cl}. Special attention is given to how the solution changes with increased resolution and layer count in the model.

The ability to reliably simulate large-scale flow structures over extended time periods is essential for understanding planetary climate systems [1]. Such simulations inform decisions related to climate adaptation and mitigation of its consequences. A major difficulty in this area arises from the wide spectrum of spatial and temporal scales present in geophysical flows. The quasi-two-dimensional character of the flow supports an inverse energy cascade, where small-scale eddies merge to form larger coherent structures [5].

A common limitation in traditional numerical models lies in the need to parameterize submesoscale processes, often due to limited computational resources or stability considerations. These parameterizations introduce additional complexity and may reduce predictive accuracy [36, 28]. Consequently, there is a growing interest in structure-preserving numerical methods that maintain the essential physical properties of the system over long integration times without the need for such approximations. Recent advances have demonstrated the effectiveness of such methods for single-layer barotropic models [7, 10], particularly those that exploit the Lie–Poisson structure of the equations. These discretizations conserve key invariants, enabling simulations that remain stable and physically consistent without external regularization. Their effectiveness has been demonstrated in reproducing energy spectra typical of two-dimensional turbulence [6], as well as in capturing the fundamental dynamics of large-scale QG flows [10].

The present paper aims to broaden the scope of these structure-preserving approaches by applying them to multi-layer QG systems. These models offer a more detailed depiction of atmospheric and oceanic dynamics by including vertical stratification in density, pressure, and flow fields [30]. Extending geometric techniques to such multi-layer configurations marks an important step toward modeling complex interactions between different atmospheric or oceanic layers [11]. We particularly study the dependency of the achievable accuracy on the layerwise resolution N and the number of layers M.

The remainder of this paper is structured as follows. Section 2 introduces the multilayer QG model and the numerical methods employed. The numerical methods and the computational settings are outlined in Section 3. Section 4 presents the dependencies of the evolution of the jets that form on spatial resolution, followed by an in-depth discussion of the critical latitude predictions. Concluding remarks are provided in Section 5.

2. Multilayer quasi-geostrophic computational model.

It was independently shown by [26] and [32] that a single-layer QG model for flow on the sphere can be derived from shallow water models by a solenoidal partitioning of the flow. This partitioning provides an alternative to the traditional partitioning into geostrophic and an ageostrophic components, which is ill-defined at the equator. Instead, the solenoidal partitioning yields a QG model suitable for the entire sphere. This model also makes it possible to incorporate multiple layers representing vertical variations in buoyancy. In this way, internal baroclinic modes can be accounted for, basic to the study of baroclinic instabilities [23, 25].

The multi-layer QG equations on the sphere are based on the Boussinesq primitive equation (PE) to which an approximate quasi-geostrophic balance is imposed under stable stratification. As discussed in detail in [11, 12], the potential vorticity q is governed by the stratified QG equations on the sphere

$$\frac{\mathrm{D}q}{\mathrm{D}t} = 0 \quad \text{where} \quad q = \mathrm{Ro}\,\nabla^2\psi + f + \mathrm{Ro}\left(\frac{L}{L_d}\right)^2 f^2 \frac{\partial}{\partial r}\left(\frac{1}{N^2}\frac{\partial\psi}{\partial r}\right) \tag{1}$$

Here, ψ is the streamfunction, f is the Coriolis parameter, Ro is the Rossby number (the ratio of typical velocity scale over the inertial velocity scale), L is a typical horizontal length scale, L_d is the Rossby deformation radius, and N is the Brunt-Väisälä frequency.

The potential vorticity for the stratified QG equations is materially conserved on planes of constant radius. It is the single prognostic variable in the model. This formulation is similar to the traditional stratified QG equation on a Cartesian plane, except for the crucial appearance of the fully latitude-dependent Coriolis term f, which also plays a role in the stratification. The geostrophic velocity can be reconstructed from the stream function ψ. The derivation of these QG equations sheds some light on the conditions under which this model can be applied. Starting from the Boussinesq PE on the sphere, the geostrophic balance is used to derive the leading-order dynamics in terms of the Rossby number. This is valid at all latitudes where a scale separation exists between the Coriolis force and inertial forces. Thus, it provides a continuous model for both mid-latitude and polar dynamics. At a narrow band around the equator, scale separation no longer holds as the Coriolis parameter vanishes. In this region, gravity waves play an important role with their own dynamics [30].

From the continuous equations in (1), a layered computational model may be inferred by subdividing the domain into concentric layers. Within each layer, a constant density may be set such that the density distribution over the layers approximates the continuous average stratification of the full 3D formulation. This is equivalent to employing a standard second-order finite-difference discretization in the radial direction [31]. When the average density stratification is stable, its level sets (isopycnals, i.e., surfaces of constant density) form non-overlapping slices of the fluid column. In the derivations above, we assumed that density fluctuations are small compared to the average stratification, indicating that the isopycnals form approximately spherical shells. Thus, we describe the fluid using several layers of constant thickness and uniform density given by the average stratification, whose level sets correspond to isopycnals of the continuous model. We divide the domain in the radial direction into M spherical shells, denoted from top to bottom with an index $j = 1, \ldots, M$. Each layer has a thickness $H_j = r_{j+1/2} - r_{j-1/2}$ with $r_{j-1/2} = (r_j + r_{j-1})/2$ such that $\sum_{j=1}^{M} H_j = H$, with H corresponding to the entire fluid layer considered. In this paper, we concentrate on the troposphere, which is the lowest layer in the Earth's atmosphere. The height of the troposphere varies across the Earth, from up to 18 km near the Equator to about 11 km at middle latitude and 6 km in the polar regions. We focus on a troposphere with a fluid layer of about 10 km as advised in [33]. Within this troposphere, most of the jet flow that forms in the Earth's boundary layer is taking place. We describe the dynamics in each layer by its potential vorticity q_j and stream function ψ_j.

A second-order centred finite difference scheme to discretize the radial derivatives in (1), similar to the approach taken in [31] for the β-plane equations, yields

$$\frac{\partial}{\partial r}\left(\frac{1}{N^2}\frac{\partial \psi}{\partial r}\right) \approx \frac{1}{H_j}\left(\frac{1}{N^2_{j+\frac{1}{2}}}\frac{\psi_{j+1}-\psi_j}{H_{j+\frac{1}{2}}} - \frac{1}{N^2_{j-\frac{1}{2}}}\frac{\psi_j - \psi_{j-1}}{H_{j-\frac{1}{2}}}\right), \tag{2}$$

where $H_{j+\frac{1}{2}} = r_{j+1} - r_j$ and the Brunt-Väisälä frequencies $N(r)$ are given by central differencing of

$$N^2(r) = -\frac{g}{\rho_0}\frac{\partial \rho}{\partial r}, \tag{3}$$

which represents the oscillation frequency of a displaced fluid parcel in a density gradient. Discretely, this is approximated as

$$N^2_{j+\frac{1}{2}} = -\frac{g}{H_{j+\frac{1}{2}}}\frac{\rho_{j+1}-\rho_j}{\rho_0} = -\frac{g'_{j+\frac{1}{2}}}{H_{j+\frac{1}{2}}} \tag{4}$$

where the reduced gravity

$$g'_{j+\frac{1}{2}} = g\frac{\rho_{j+1}-\rho_j}{\rho_0} \tag{5}$$

has been introduced as a measure of the effective gravitational acceleration between layers.

If we apply the central discretization in the radial direction to the stratified QG equations (1), we find the multi-layer QG equations on the sphere

$$\dot{q}_j + \{\psi_j, q_j\} = 0, \quad j = 1, \ldots, M, \tag{6}$$

where q_j is the layer-wise potential vorticity, given in vector form as

$$\mathbf{q} = \nabla^2 \boldsymbol{\psi} + \mathbf{f} + A\boldsymbol{\psi}, \tag{7}$$

where $\mathbf{q} = [q_1, q_2, \ldots, q_M]^T$ is a vector containing the layerwise PV, and similarly $\boldsymbol{\psi} = [\psi_1, \psi_2, \ldots, \psi_M]^T$ and $\mathbf{f} = [1, 1, \ldots, 1]^T f$. The interaction between layers is given by the matrix $A \in \mathbb{R}^{M\times M}$. In terms of the reduced gravity and layer thicknesses, the matrix A may be expressed as

$$A = \mathrm{Ro}\left(\frac{L}{L_d}\right)^2 f^2 \begin{bmatrix} -\frac{1}{g'_{3/2}H_1} & \frac{1}{g'_{3/2}H_1} & 0 & 0 & \ddots & 0 \\ \frac{1}{g'_{3/2}H_2} & -\frac{1}{g'_{3/2}H_2} - \frac{1}{g'_{5/2}H_2} & \frac{1}{g'_{5/2}H_2} & 0 & \ddots & 0 \\ 0 & \frac{1}{g'_{5/2}H_3} & -\frac{1}{g'_{5/2}H_3} - \frac{1}{g'_{7/2}H_3} & \frac{1}{g'_{7/2}H_3} & \ddots & 0 \\ \vdots & \ddots & \ddots & \ddots & \ddots & \vdots \\ 0 & \cdots & \cdots & \cdots & \cdots & -\frac{1}{g'_{M-1/2}H_M} \end{bmatrix} \tag{8}$$

as follows directly from (1) using (2) and (4). For a general interaction matrix A, an implicit time-step involves solving a system of coupled elliptic equations. If the matrix A is diagonalizable an ideal preconditioner for the coupled system can be devised, which has clear computational benefits, we discuss this in more detail in the next section. The material derivative $\mathrm{D}/\mathrm{D}t$ has been rewritten using the canonical Poisson bracket on the sphere, which, in terms of the latitude ϕ and the longitude θ, is given by

$$\{a, b\} = \frac{1}{R^2\cos\phi}\left(\frac{\partial a}{\partial\theta}\frac{\partial b}{\partial\phi} - \frac{\partial a}{\partial\phi}\frac{\partial b}{\partial\theta}\right) = (\hat{\mathbf{r}}\times\nabla a)\cdot\nabla b. \tag{9}$$

where R is the radius of the sphere. From this formulation of horizontal PV transport in terms of the canonical Poisson bracket on the sphere, we note the layerwise similarity to the single-layer QG equation as described on the sphere by [32] and [26]. In particular, the only difference appears in the relation between the stream function and potential vorticity (7).

Recently, the Poisson structure of the single-layer QG equation on the sphere has been discussed in [19]. From their analysis, we find that (6) constitutes a Lie–Poisson system on the space of smooth functionals on the sphere $\mathcal{C}^\infty(\mathcal{S}^2)$ for each layer separately, where the Lie–Poisson bracket is given in terms of the canonical Poisson bracket by

$$\{\mathcal{A}, \mathcal{B}\}_{LP}(q) = \int_{\mathcal{S}^2} q\left\{\frac{\delta\mathcal{A}}{\delta q}(q), \frac{\delta\mathcal{B}}{\delta q}(q)\right\}\mathrm{d}x, \tag{10}$$

with $\mathcal{A}, \mathcal{B} : \mathcal{C}^\infty(\mathcal{S}^2) \to \mathbb{R}$ smooth functionals and $\mathrm{d}x$ an infinitesimal area element, which in latitude-longitude coordinates is given by $\mathrm{d}x = R\cos\phi\,\mathrm{d}\phi\,\mathrm{d}\theta$. The variation δ is taken in the Gateaux sense, which uniquely defines the variational derivatives $\delta\mathcal{A}/\delta q$ and $\delta\mathcal{B}/\delta q$. The advection of layer-wise PV (6) may thus be more generally written as

$$\frac{\mathrm{d}}{\mathrm{d}t}\mathcal{F}(q_j) = \{\mathcal{F}(q_j), \mathcal{H}(q_j)\}_{LP}, \tag{11}$$

with $\mathcal{F} \in \mathcal{C}^\infty(\mathcal{S}^2)$ any smooth functional and the Hamiltonian functional given by

$$\mathcal{H}(q) = -\frac{1}{2}\sum_{j=1}^{M}\int_{\mathcal{S}^2}\psi_j(q_j - f)\,\mathrm{d}x \tag{12}$$

Thus, similar to the single-layer QG equations, this system allows for infinitely many conserved quantities in the form of Casimir functionals $\mathcal{C} : C^\infty(\mathcal{S}^2) \to \mathbb{R}$ for which it holds that

$$\{\mathcal{F}(q_j), \mathcal{C}(q_j)\}_{LP} = 0, \quad \forall\mathcal{F} : C^\infty(\mathcal{S}^2) \to \mathbb{R}, \tag{13}$$

Here, this results in $\mathcal{C}(q_j) = \int_{S^2} \zeta(q_j)\mathrm{d}x$ for any smooth analytic function $\zeta \in C^\infty(\mathbb{R})$, which indicates that for each layer, any integrated function of potential vorticity is a constant of motion. This may be verified by direct computation. Typically, only integrated monomials of PV are considered since they form a basis for functions on the sphere. In particular, the integrated square of PV is called the total enstrophy and plays an important role in the characterization of turbulence in geophysical fluid dynamics [24, 13]. As previously noted in [10], this conservative property is independent of the specific relation between the stream function and potential vorticity. This explains the similarity in the constants of motion between this model and other incompressible 2D flows, such as the 2D Euler equations and the rotating shallow water equations. For a detailed overview of the relation between these models, we refer to [17].

In the next section, we present the spatial discretization that was used, closely following [38].

3. **Numerical method for resolving turbulent jet flow on the sphere.** In the previous section, the multi-layer QG equations on the sphere were specified, resulting in a dynamical system governing the potential vorticity q, in terms of the stream function ψ. In this section, we detail the numerical method for solving this system. This approach comes in two steps. First, we project functions on the sphere onto a particular discrete basis such that the resulting system of ODEs is Lie–Poisson. Then, a suitable time integrator is selected to conserve the Casimirs of the discrete system as well as the associated Hamiltonian energy.

Spatial discretization and streamfunction. The construction of a projection of the infinite-dimensional Lie–Poisson system (11) onto a finite-dimensional Lie–Poisson system on the sphere was first employed in [38]. This was motivated by a projection method on a flat geometry in [37] for the 2D Euler equations. The projection method corresponds to a finite-dimensional approximation of the Lie–Poisson bracket, which can be written as a matrix algebra of dimension $(N \times N)$. Here, as before, N denotes the number of computational degrees of freedom per layer. As $N \to \infty$, the convergence of the method involves a sequence of Lie algebras that approaches the infinite-dimensional Poisson algebra $\mathcal{C}^\infty(\mathcal{S}^2)$ such that the structure constants of the matrix bases converge to those of the spherical harmonics basis $Y_{l,m}$ of $C^\infty(\mathcal{S}^2)$. As was shown for a general case in [2], and later for the spherical geometry by [38] based on the work of [15], such a sequence exists, given by the basis $T_{l,m}$ for the matrix Lie algebra $\mathfrak{u}(N)$, i.e., the algebra of skew-Hermitian matrices. Given a function $a \in C^\infty(\mathcal{S}^2)$ written in terms of the basis as $a = \sum_{l=0}^{\infty}\sum_{m=-l}^{l} a_{l,m}Y_{l,m}$, the implied projection $\Pi_N : \mathcal{C}^\infty(\mathcal{S}^2) \to \mathfrak{u}(N)$ is then given by

$$\Pi_N a := \sum_{l=0}^{N-1}\sum_{m=-l}^{l} i a_{l,m}\hat{T}_{l,m}, \tag{14}$$

where the modified basis $\hat{T}_{l,m}$ follows directly from the complex part of $T_{l,m}$ as detailed in [7]. The $\hat{T}_{l,m}$ are eigenfunctions of the discrete Laplace operator on the sphere Δ_N as provided by [16].

The similarity between the structure constants of the discrete basis T_{lm} and those of Y_{lm} in the continuous case also results in a close relation between the Poisson bracket (9) and the Lie bracket on $\mathfrak{u}(N)$, which is the matrix commutator.

Specifically, we have

$$\Pi_N\{f,g\} = [\Pi_N f, \Pi_N g]_N + \mathcal{O}(N^{-2}), \tag{15}$$

where $[A,B]_N = N^{3/2}/\sqrt{16\pi}\,(AB - BA)$ is the rescaled matrix commutator [2, 3]. As established in [20] (Table 1), we have that

$$\lim_{N\to\infty} \frac{4\pi}{N}\mathrm{Tr}(f(-iW)) = \int_{S^2} f(\omega)\mu(dx). \tag{16}$$

for a general differentiable function f, evaluated in terms of a matrix W. In our applications, W is typically the vorticity matrix. The integral over the sphere S^2 contains the Lebesgue measure $\mu(dx)$, At given N, the expressions on the left- and right-hand sides do not coincide for general f, but for monomials up to order $N-1$, the difference between the corresponding Casimir of the original system and the Casimir of the discrete system is constant in time [15]. Correspondingly, at given N, the discrete LP system has the maximum number of analogous Casimirs.

Using the explicit projection in (14), we may introduce the layer-wise potential vorticity matrices Q_j and associated stream matrices P_j through

$$Q_j = \sum_{l=0}^{N-1}\sum_{m=-l}^{l} i(q_j)_{lm}\hat{T}_{lm}^{(N)}, \quad \text{and} \quad P_j = \sum_{l=0}^{N-1}\sum_{m=-l}^{l} i(\psi_j)_{lm}\hat{T}_{lm}^{(N)}, \quad j = 1,\ldots,M. \tag{17}$$

where i is the imaginary unit $i^2 = -1$. Similarly, we introduce the Coriolis matrix $F := \Pi_N f$ and its square $S := \Pi_N f^2$, which enables to derive the spatial discretization of (6) as

$$\dot{Q}_j = -[P_j, Q_j] \quad j = 1,\ldots,M \tag{18}$$

The potential vorticity is given in terms of the stream matrices as

$$Q_j = \Delta_N P_j + F + \tilde{S} \circ \left(\sum_{k=1}^{M} A_{jk} P_k\right) \quad j = 1,\ldots,M \tag{19}$$

where the projection of the product $f^2\psi$ is given by the operation $\tilde{S}\circ P$ with $\circ$ denoting element-wise multiplication, as was derived in [10]. The matrix $\tilde{S}$ is given by

$$\tilde{S}_{ij} = -\frac{i}{2}\sqrt{\frac{N}{4\pi}}(S_{ii} + S_{jj}). \tag{20}$$

System (18) constitutes M isospectral equations. They are Lie–Poisson with respect to the Lie algebra $\mathfrak{u}(N)$ with the Lie bracket $[\cdot,\cdot]$, for which the Casimirs $C_{j,k}$ by isospectrality are given as

$$C_{j,k} = \mathrm{trace}\left((Q_j)^k\right), \quad k = 0,1,\ldots,N-1, \quad j = 1,\ldots,M, \tag{21}$$

which indicates that integrated monomial functions of potential vorticity are conserved in each layer, similar to the dynamics of a single-layer QG model.

Solving the system of equations (18) requires a suitable time integration method, as well as a method for calculating the stream matrices P_j from the implicit relation given in (19). This is discussed next, closely following [11, 12]. Since the main dynamical variable in the evolution of multi-layer quasi-geostrophic flow is the potential vorticity, the resulting velocity field, which in turn is calculated from the stream function, must be determined using the implicit relation (19). Under the influence of density stratification, the fully coupled system (19) needs to be considered. For a general interaction matrix, this involves solving a system of M

coupled elliptic equations of size $N \times N$. However, in many cases, the matrix A is diagonalizable, leading to an ideal preconditioner for the coupled system. In fact, if the matrix A is diagonalizable, there exists an invertible square matrix V and a diagonal matrix D such that

$$A = VDV^{-1}. \tag{22}$$

Substitution of this decomposition into (19) then gives

$$\hat{Q}_k = \Delta_N \hat{P}_k + F + \tilde{S} \circ \left(D_{kk} \hat{P}_k \right), \quad k = 1, \ldots, M, \tag{23}$$

where $\hat{Q}_k = \sum_{j=1}^{M} V_{kj}^{-1} Q_j$ and $\hat{P}_k = \sum_{j=1}^{M} V_{kj}^{-1} P_j$ are the potential vorticity matrices and stream matrices respectively corresponding to the modes of system [29]. Crucially, the potential vorticity matrix $\hat{Q}_j$ associated with a particular mode j is independent of the other modes. Thus, system (23) constitutes M independent implicit equations for the stream matrices $\hat{P}_j$, which can be made explicit as the solution to

$$\hat{P}_k = \left(\Delta_N + D_{kk} \tilde{S} \circ \right)^{-1} (\hat{Q}_k - F), \quad k = 1, \ldots, M, \tag{24}$$

An efficient method using $\mathcal{O}(N^2)$ operations is obtained by adopting diagonal splitting as developed in [10]. The layer-wise PV and stream function matrices can then be reconstructed using the relations

$$Q_j = \sum_{k=1}^{M} V_{jk} \hat{Q}_k, \quad P_k = \sum_{k=1}^{M} V_{jk} \hat{P}_k \tag{25}$$

If the interaction matrix A is not diagonalizable, the stream matrices can still be calculated from (19) using diagonal splitting. If we denote the mth diagonal of a matrix by the superscript $\cdot^{(m)}$ as a row vector, we may introduce the column vectors $P^{(m)}, Q^{(m)} \in \mathbb{C}^{(N-|m|)L}$ as

$$\mathbb{P}^{(m)} = \begin{bmatrix} P_1^{(m)} & P_2^{(m)} & \cdots & P_L^{(m)} \end{bmatrix}^T \tag{26}$$

and

$$Q^{(m)} = \begin{bmatrix} Q_1^{(m)} & Q_2^{(m)} & \cdots & Q_L^{(m)} \end{bmatrix}^T, \tag{27}$$

which enables to decompose the entire system (19) into its diagonals as

$$(\mathbb{L}^{(m)} + \mathbb{S}^{(m)}) P^{(m)} = Q^{(m)} - F^{(m)}, \quad m = -(N-1), \ldots, N-1 \tag{28}$$

using the matrix operators $\mathbb{L}^m, \mathbb{S}^m \in \mathbb{C}^{[(N-|m|)M] \times [(N-|m|)M]}$ given as

$$\mathbb{L}^{(m)} = I_M \odot \Delta_N^{(m)} \tag{29}$$

and

$$\mathbb{S}^{(m)} = A \odot \tilde{S}^{(m)} \tag{30}$$

where $\odot$ denotes the Kronecker product and I_M is the identity matrix of dimension M. The matrix $(\mathbb{L}^{(m)} + \mathbb{S}^{(m)})$ is extremely sparse with only 5 nonzero diagonals following from the definition of the Laplacian and equation (**??**). These can be solved efficiently using appropriate pre-conditioners [4] or using iterative methods. Here, we note that in the case of a diagonalizable matrix A, the preconditioner can be found from the decomposition (22), which leads directly to system (24). Note that one needs only to solve for the diagonals $m \geq 0$, since the matrices P_j are skew-Hermitian. The linear scaling of the computational complexity with the number of layers facilitates simulations at high horizontal resolutions, similar to previous work on barotropic QG flow as reported by [10]. These computational characteristics were measured on a MATLAB implementation of the computational model, as discussed momentarily.

Time integration method. The evolution of the dynamical system is carried out by solving equation (18) in time. Analogous to the conservation of integrated functions of potential vorticity in the continuous system, this system of ODEs preserves the trace of polynomial functions of Q_j up to polynomial order $(N-1)$ as indicated in equation (21) for each layer. This property is equivalent to the spectrum of the layerwise potential vorticity matrix being conserved [35], indicating that the evolution in (18) is iso-spectral. This property is similar to the isospectral evolution of the potential vorticity matrix in a single-layer QG model as in [10], where it was also remarked that the isospectral property holds independent of the choice of the advecting stream matrix. Therefore, we can select the same time-integration method as used for the single-layer model to conserve the matrix spectrum on a discrete level.

We employ the time integrator as formulated in [21], based on second-order symplectic midpoint integration. This integrator falls within the class of IsoSyRK methods, which are both symplectic and isospectral [22]. Given the solution Q_j^n at time t_n, the solution of (18) at time $t_{n+1} = t_n + h$ can then be written as follows:

$$\begin{cases} \tilde{Q}_j = Q_j^n + \frac{h}{2}\left[P_j, \tilde{Q}_j^n\right] + \frac{h^2}{4} P_j \tilde{Q}_j P_j \\ Q_j^{n+1} = \tilde{Q}_j + \frac{h}{2}\left[\tilde{P}_j, \tilde{Q}_j\right] - \frac{h^2}{4} \tilde{P}_j \tilde{Q}_j \tilde{P}_j, \end{cases} \tag{31}$$

where $\tilde{P}_j$ is the stream matrix corresponding to the potential vorticity matrix $\tilde{Q}_j$ as given by equation (19). The integration thus consists of two steps. The first equation gives an implicit relation for the intermediate step $\tilde{Q}_j$, which is solved using fixed point iteration. This creates a sequence $\left\{\tilde{Q}_j^k\right\}$ with $\tilde{Q}_j^0 = Q_j^n$. The time step h is chosen sufficiently small such that the sequence converges to $\tilde{Q}_j$ as $k \to \infty$. This contraction can be performed in parallel for each layer, with each process terminating when the sequence has converged to within a set tolerance. For the chosen time step sizes h, the L_∞ norm of $\tilde{Q}_j^{k+1} - \tilde{Q}_j^k$ typically reaches $\mathcal{O}(10^{-10})$ after only 4 or 5 iterations. After sufficient convergence, the stream matrices $\tilde{P}_j$ are calculated, and a full time step is completed by evaluating the right-hand side in the second equation in (31).

4. **Jet flow induced on rotating sphere.** In this section, we demonstrate the capabilities of the developed numerical method by simulating a geophysical flow model in an Earth-like configuration. We specify the details and relevant parameters in Subsection 4.1 and present the structured jet flow forming in a model of the troposphere (approximately the first 10 km above the Earth's surface), up to the stratosphere (approximately the next 40 km). The simulations start from an initially random condition as described in Subsection 4.2. We consider a reference four-layer QG simulation and show the convergence characteristics upon grid refinement. Convergence characteristics upon increasing the number of layers covering the stratosphere are discussed in Section 4.3.

4.1. **Simulation set-up.** To investigate the multi-layer jet flow that forms in the troposphere on a rotating Earth-like planet, we incorporate the average stratification of the mass density to represent the reduced gravity in the various layers. A model often used for the average density stratification proposes that

$$\rho(h) = \rho_0 e^{-h/H} \tag{32}$$

where the reference mass density is taken at atmospheric conditions on the Earth's surface $\rho_0 = 1.225\ kg/m^3$, h denotes the altitude and H is a reference scale for the troposphere, here taken as $H = 10\ km$. Physically, temperature drops with altitude, which affects density, as documented in [9]. The exponential model for the mass density implies a reduced gravity distribution given by

$$g_i' = g_0\Big(\exp(-(1-\frac{i}{M})) - \exp(-(1-\frac{i-1}{M}))\Big)\ ;\ i = 1, ..., M \tag{33}$$

for the ith layer in an M layer model. Here, $g_0 = 9.80665\ m/s^2$ at sea level. The radius of the Earth is taken as $R = 6.378\ 10^6\ m$.

The simulations adopt Zeitlin truncation, which, through its structure-preserving nature, conserves Casimirs of the system as well as energy and enstrophy. To verify the structure-preserving properties of the numerical methods, we perform a simulation of geostrophic flow in the absence of forcing, dissipation and friction. This enables full-scale computations of M-layer models, without the need to introduce regularizing eddy-dissipation or explicit forcing [11]. Instead, the simulations start from a randomly generated, structureless initial flow and concentrate on the spontaneous formation of structured solutions displaying a pattern of jets across the sphere and over all layers. The spatial resolution per layer may be specified separately; in our simulations we consider $N = 48, 64, 96, 128, 192, 256$, and adopt a tolerance of 10^{-10} for the fixed point iteration. Typically, full convergence is observed after 4 to 5 cycles. As a point of departure, we look into a reference problem with 4 layers, each of 2500 m height.

4.2. **Jet structuring in four-layer reference model.** In Figure 1, the velocity field in the four layers is shown after 1000 simulated days, at a spatial resolution of $N = 256$ degrees of freedom per layer. The solution shows relatively large differences, of about a factor 3, in typical amplitudes across the layers. This poses a challenge to the visualization. When using a single color bar for all four layers simultaneously, rather poor contrast emerges in some of the figures. This makes the structuring of the flow much less visible. Instead, by concentrating on qualitative features, and correspondingly selecting appropriate color ranges per figure, we can clearly express the main structure in the solution for the different layers. To appreciate the qualitative structuring in the flow, we therefore adhere to multiple color bars, which appears adequate for the interpretation of the flow. In fact, the figures display a remarkable structure emerging from the initially random state, displaying smooth features of similar scales across the layers. The flow structures appear somewhat elongated in the circumferential direction. This characteristic appears over all layers and is slightly more pronounced near the equator. Layers that are higher up in the atmosphere show a decreased velocity field by a factor of about 3 in this model configuration. The statistically steady state forms after a short transient of about 250 days, as may be inferred from Figure 2(a), where the evolution of the total kinetic energy per layer is depicted. From the evolving kinetic energy, we also notice a strong reduction in the intensity of the flow when considering layers further away from the Earth's surface; the average kinetic energy in the statistically steady state decreases by a factor of about 3 relative to the kinetic energy in the most

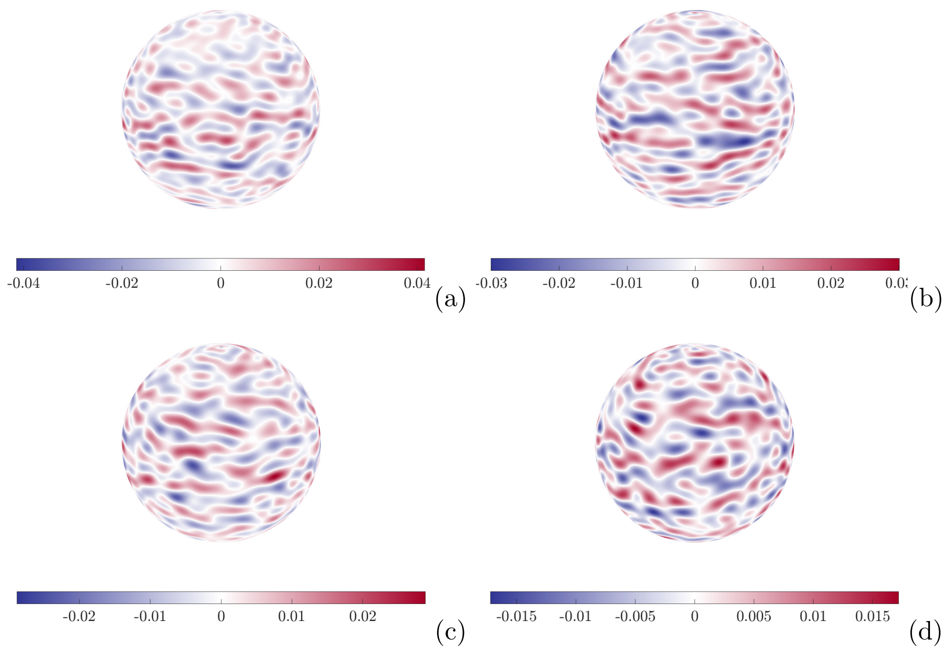

FIGURE 1. Instantaneous velocity fields at $N = 256$ for the reference four-layer QG-model of the troposphere from the bottom to the top layer (a-d) after 1000 simulated days. Note that the amplitude of the flow structures decreases with increasing height of the layer; this is expressed by selecting different color-bars.

energetic first layer. The numerical method was found to conserve Casimirs within $O(10^{-8})$ relative variations, as was also established in [11].

The computing time associated with the Zeitlin method as described in [11] is observed in Figure 2(b). The implementation was realized in MATLAB, and the simulations were executed on a laptop running on an Apple M2 Max processor. The computing time is seen to scale approximately quadratically with N, for full simulations including initialization, time-stepping, and on-the-fly post-processing. This scaling behavior is already well-established at modest resolutions of $N = 48$, and appears to be maintained also for the higher resolutions considered here. In [7], a turbulent, forced geophysical flow on an 'aquaplanet' was considered at elevated resolutions of $N = 1024, ..., 4096$. This study indicated $T \sim N^3$, as motivated primarily by the complexity of matrix multiplications. The cubical scaling is complemented here with a more favorable scaling of $T \sim N^2$ which appears to hold at the much more modest resolutions needed to capture the smooth structures in our 'atmospheric' planet model. The scaling of the main calculation steps is mixed with the scaling of various other steps, e.g., post-processing and time stepping, in a full simulation, which turns out closer to $T \sim N^2$. More attention will be given in the future to investigate the effective scaling with N of our computational model.

The kinetic energy spectrum at $N = 48$ is compared to that obtained at $N = 256$ in Figure 3. We observe a close correspondence between the two spectra in the statistically steady state. The smaller scales at $N = 256$ are of course absent at

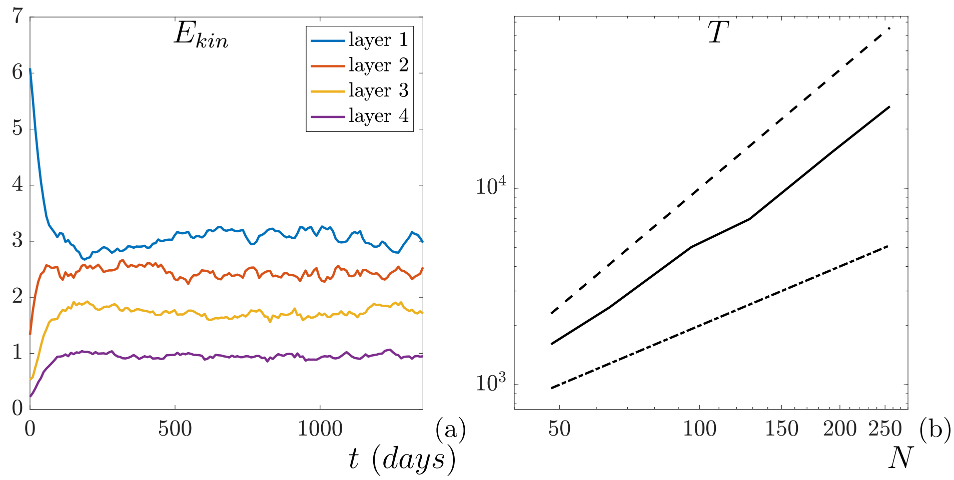

FIGURE 2. (a): Developing kinetic energy E_{kin} across the four layers of the reference model from bottom to top represented by layer 1 to layer 4, at a resolution per layer of $N = 256$ modes. The initial random state rapidly forms a statistically steady time-dependent solution in about 250 days; (b) Scaling of computational time T (in seconds, using a modern laptop) with the number of degrees of freedom N per horizontal layer. The measured simulation times are compared with linear (dash-dot) and quadratic (dash) scaling with N, illustrating $T \sim N^2$.

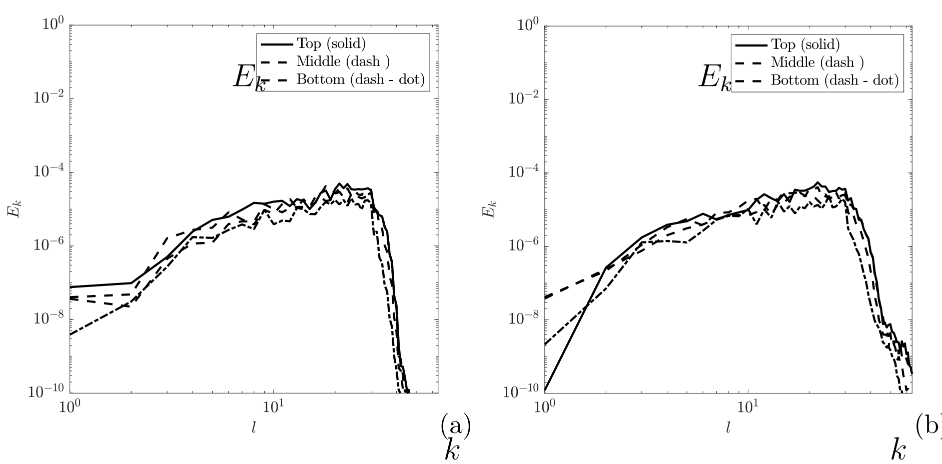

FIGURE 3. Kinetic energy spectrum in the fully developed state after 1000 days, comparing results at $N = 48$ (a) with $N = 256$ (b). The bottom layer (solid) and the top layer (dash-dot) roughly provide an envelope for the spectrum of the two inner layers (dash).

the coarser resolution and contribute to specific features in the flow. Otherwise, the general appearance of, e.g., the velocity field is remarkably similar at both resolutions, indicating that the Zeitlin truncation method, which is essentially a structure-preserving spectral-like discretisation method, shows high fidelity also at modest resolutions for our 'atmospheric' Earth model.

4.3. **Convergence of critical latitude predictions.** The critical latitude ϕ_{cl} is the latitude at which the ratio between the Rossby deformation scale L_D and the Rhines scale L_R equals 1, i.e.,

$$\frac{L_D}{L_R} = 1 \;\rightarrow\; \phi_{cl} \tag{34}$$

The ratio is also called the nonlinearity parameter for QG flow, as it measures the relative strength of the nonlinear advection term compared to hydrostatic and Coriolis effects.

In this subsection, we first consider effects of spatial resolution on the accuracy with which the critical latitude can be determined. Subsequently, we investigate the convergence of the critical latitude upon increasing the number of layers in the troposphere model.

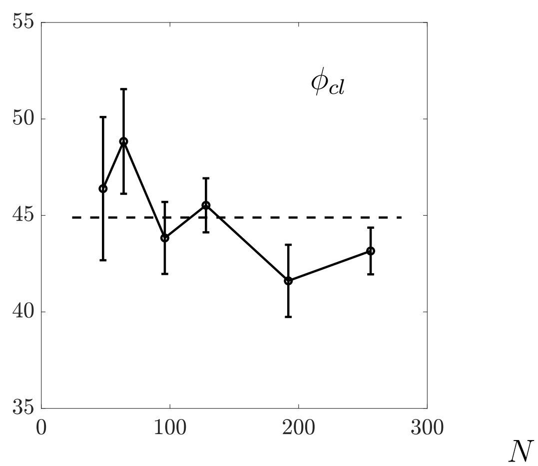

FIGURE 4. Median of the critical latitude ϕ_{cl} of the reference four-layer system computed by averaging over 96 velocity fields, at different spatial resolutions 48-64-96-128-192-256. Averaged over all resolutions (dashed line), a value of ≈ 44.9 degrees is found. The uncertainty in ϕ_{cl} is expressed in terms of the interquartile range (IQR) shown as error bar. Overall, the accuracy with which the different randomly initiated simulations can be averaged over corresponds to an IQR of about 3 % for the three highest resolutions.

Convergence: Spatial resolution. In Figure 4, the estimated critical latitude in the reference four-layer model is shown as a function of the spatial resolution N, averaged over 96 solutions and 5 independently initiated simulations. The critical latitude is determined by its median, which is found at about 44.9 degrees with an uncertainty expressed by the interquartile range (IQR) of about 3 % for the three highest resolutions. The uncertainty is not only related to differences in the spatial resolution, but also to the width of the time-averaging window that was used in the calculation, and the differences in the random initial condition. The latter implies small differences in the initial total kinetic energy, which, because of the structure-preserving nature of the numerical method, persist throughout the entire simulation. Hence, although the critical latitude can be determined robustly across different resolutions, it cannot be found with very high accuracy, due to the variations in the obtained solutions. To further quantify the convergence with increasing spatial resolution N, a classical deterministic analysis based on a single function describing the initial condition can be incorporated.

Convergence: Number of layers. Finally, we consider the effect of varying the number of layers spanning the troposphere. Until now, we have focused on a four-layer model to investigate the performance of the numerical methods. Now, we want to vary this number and infer whether higher resolution in the radial direction is beneficial for predicting the flow and the corresponding critical latitude.

A clear qualitative impression of the effect of properly resolving the dynamics across the layers may be inferred from Figure 5. At $N = 96$, an increase in the number of layers M from 1, 2, 4, ..., 32 is seen to yield an ever more refined flow structure nearer the equator. The jet-like structures in the flow are more pronounced and slender with increasing M, while nearer the poles, a smoother velocity field develops at larger M.

The striking qualitative effect of increasing the number of layers M in the model also expresses itself in other flow features, such as the critical latitude. In Figure 6, we observe a significant, almost linear decrease in the critical latitude with increasing number of layers in the troposphere. Further increasing M is expected to yield further reduction in ϕ_{cl}, corresponding to the already mentioned increased dynamic activity near the equator. To make definite statements on the limit solution at large M, more simulations are needed. Future research should be dedicated to this to infer the quality of QG predictions that include explicit layer coupling in the radial direction. Moreover, the effects of more refined layer coupling in the troposphere may be investigated to assess the physical relevance of the simulated solutions.

5. **Conclusion and outlook.** In this paper, we presented a global formulation for the multilayer quasi-geostrophic (QG) equations and applied a corresponding Casimir-preserving numerical method to simulate the dynamics. By extending the baroclinic QG models from traditional local f-plane or β-plane approximations to a global spherical framework, we provide a comprehensive tool for studying large-scale atmospheric and oceanic dynamics. The numerical method is based on similar global methods for the barotropic QG equations developed in [10], which in turn extends a study on the two-dimensional Euler equations in [7]. The discretization yields a finite-dimensional system which preserves all monomial Casimirs of the discrete system. Using an isospectral symplectic time integrator, we could preserve the monomial Casimirs during the simulation.

We have employed the developed method to simulate geostrophic flow in the multilayer context. We have shown that zonal jets form in a reference four-layer model, and that the solution is represented accurately already at modest resolutions N per layer, starting in the range of 96. A precise capturing of all dynamics showed the system to evolve quickly, i.e., within about 250 days, into a statistically steady state, starting from a random initial condition. The smooth part of the kinetic energy spectrum was well represented even at $N = 48$, while smaller details in the jet flow required $N = 192 - 256$ to be properly resolved on an Earth-like planet. The critical latitude was found to be approximately in the range of 44.5 ± 2 degrees,

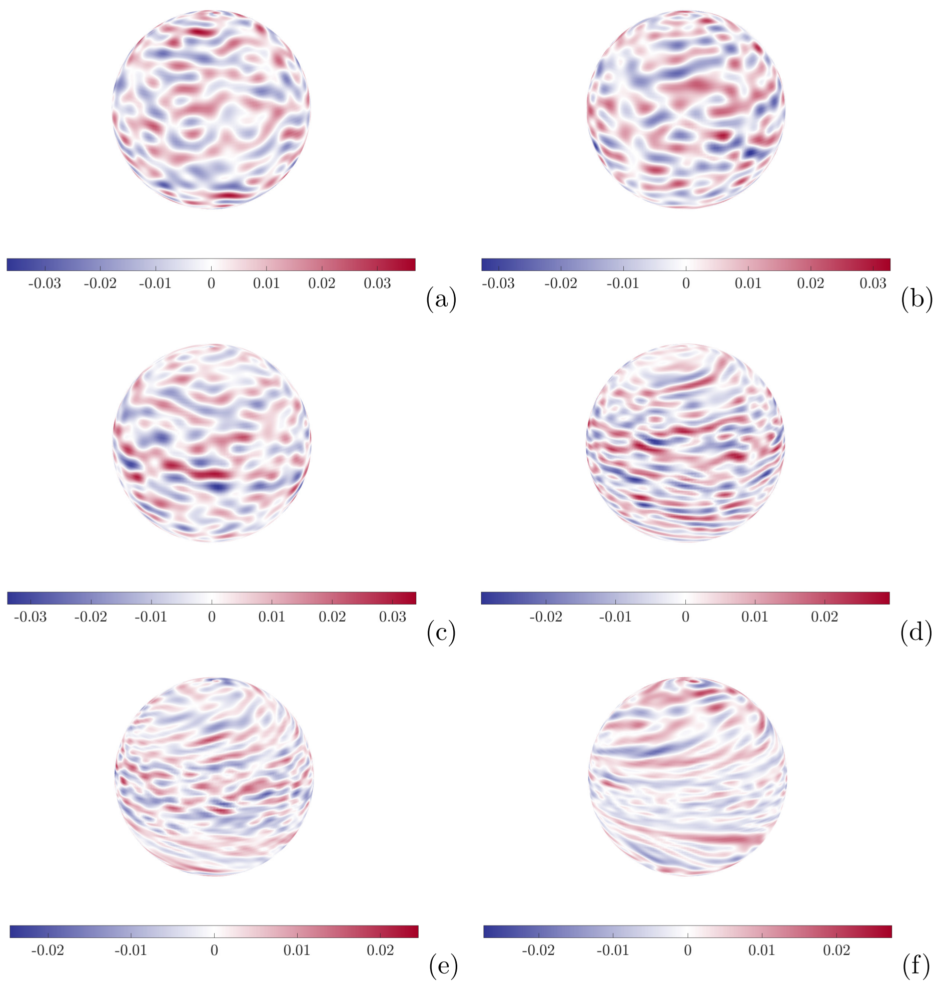

FIGURE 5. Velocity field in the first layer for models resolving the troposphere in M layers where $M = 2^k$ for $k = 0, 1, 2, ..., 5$ at $N = 96$. The results at different k are shown in figures a, b, c, ..., f, respectively.

with an uncertainty stemming from spatial resolution limitations, but also from the use of random initial conditions.

The effects of changing the number of layers in the model for the troposphere were found to be quite pronounced, expressed in striking structuring of the flow nearer the equator and a much reduced critical latitude upon increasing M. This calls for a closer consideration of the layer coupling within the troposphere, both numerically and in their physical modeling. The development of such a novel numerical framework will pave the way for application in large-scale simulations of global atmospheric and ocean dynamics. This is a topic of ongoing research.

Acknowledgments. The authors are very much indebted to Darry Holm of Imperial College London. The numerous discussions we had together helped shape the

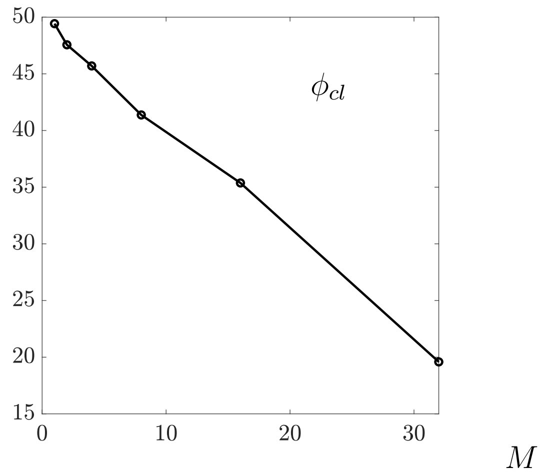

FIGURE 6. Critical latitude ϕ_{cl} as a function of the number M of layers for $M = 1, 2, 4, ..., 32$, predicted at a layerwise resolution of 96.

concepts and kept the research focused. Part of the work of the authors was generously supported by the Dutch Science Foundation (NWO) within the SPRESTO project as part of the TOP-1 granting system.

REFERENCES

[1] P. Bechtold, N. Semane and S. Malardel, Convection and waves on small planets and the real earth, in *Parameterization of Atmospheric Convection: Volume 2: Current Issues and New Theories*, World Scientific, 2016, 59-73.

[2] M. Bordemann, J. Hoppe, P. Schaller and M. Schlichenmaier, gl(∞) and geometric quantization, *Communications in Mathematical Physics*, **138** (1991), 209-244.

[3] M. Bordemann, E. Meinrenken and M. Schlichenmaier, Toeplitz quantization of kähler manifolds and gl(n), $n \to \infty$ limits, *Communications in Mathematical Physics*, **165** (1994), 281-296.

[4] K. Chen, *Matrix Preconditioning Techniques and Applications*, Cambridge Monogr. Appl. Comput. Math., 19. Cambridge University Press, 2005.

[5] S. Chen, R. E. Ecke, G. L. Eyink, M. Rivera, M. Wan and Z. Xiao, Physical mechanism of the two-dimensional inverse energy cascade, *Physical Review Letters*, **96** (2006), 084502.

[6] P. Cifani, M. Viviani, E. Luesink, K. Modin and B. J. Geurts, Casimir preserving spectrum of two-dimensional turbulence, *Physical Review Fluids*, **7** (2022), L082601.

[7] P. Cifani, M. Viviani and K. Modin, An efficient geometric method for incompressible hydrodynamics on the sphere, *Journal of Computational Physics*, **473** (2023), 111772, 10 pp.

[8] S. Ephrati, E. Jansson, A. Lang and E. Luesink, An exponential map free implicit midpoint method for stochastic lie-poisson systems, arXiv preprint, `arXiv:2408.16701`.

[9] I. O. for Standardization, *Standard Atmosphere*, ISO 2533:1975.

[10] A. D. Franken, M. Caliaro, P. Cifani and B. J. Geurts, Zeitlin truncation of a shallow water quasi-geostrophic model for planetary flow, *Journal of Advances in Modeling Earth Systems*, **16** (2024), e2023MS003901.

[11] A. D. Franken, E. Luesink, S. R. Ephrati and B. J. Geurts, Casimir preserving numerical method for global multilayer geostrophic turbulence, *Journal of Computational Physics*, **538** (2025), 114155, 17 pp.

[12] A. Franken, *Structure-Preserving Numerical Methods for Global Geostrophic Turbulence*, Phd thesis, University of Twente, Netherlands, 2024.

[13] E. Gkioulekas, The effect of asymmetric large-scale dissipation on energy and potential enstrophy injection in two-layer quasi-geostrophic turbulence, *Journal of Fluid Mechanics*, **694** (2012), 493-523.

[14] D. D. Holm, R. Hu and O. D. Street, Lagrangian reduction and wave mean flow interaction, *Physica D: Nonlinear Phenomena*, **454** (2023), 133847, 17 pp.
[15] J. Hoppe, Diffeomorphism groups, quantization, and SU(∞), *International Journal of Modern Physics A*, **4** (1989), 5235-5248.
[16] J. Hoppe and S.-T. Yau, Some properties of matrix harmonics on S^2, *Communications in Mathematical Physics*, **195** (1998), 67-77.
[17] E. Luesink, *Stochastic Geometric Mechanics of Thermal Ocean Dynamics*, Phd. Thesis, Imperial College London, 2021.
[18] E. Luesink, S. Ephrati, P. Cifani and B. Geurts, Casimir preserving stochastic lie–poisson integrators, *Advances in Continuous and Discrete Models*, **2024** (2024), Paper No. 1, 23 pp.
[19] E. Luesink, A. Franken, S. Ephrati and B. Geurts, Geometric derivation and structure-preserving simulation of quasi-geostrophy on the sphere, arXiv preprint, `arXiv:2402.13707`.
[20] K. Modin and M. Viviani, Two-dimensional fluids via matrix hydrodynamics, `arXiv:2405.14282`.
[21] K. Modin and M. Viviani, A Casimir preserving scheme for long-time simulation of spherical ideal hydrodynamics, *Journal of Fluid Mechanics*, **884** (2020), A22, 27 pp.
[22] K. Modin and M. Viviani, Lie–poisson methods for isospectral flows, *Foundations of Computational Mathematics*, **20** (2020), 889-921.
[23] N. A. Phillips, Geostrophic motion, *Reviews of Geophysics*, **1** (1963), 123-176.
[24] R. Salmon, Two-layer quasi-geostrophic turbulence in a simple special case, *Geophysical & Astrophysical Fluid Dynamics*, **10** (1978), 25-52.
[25] R. Salmon, Baroclinic instability and geostrophic turbulence, *Geophysical & Astrophysical Fluid Dynamics*, **15** (1980), 167-211.
[26] W. H. Schubert, R. K. Taft and L. G. Silvers, Shallow water quasi-geostrophic theory on the sphere, *Journal of Advances in Modeling Earth Systems*, **1** (2009), Quarter 2.
[27] T. A. Shaw, Mechanisms of future predicted changes in the zonal mean mid-latitude circulation, *Current Climate Change Reports*, **5** (2019), 345-357.
[28] I. Shevchenko and P. Berloff, Multi-layer quasi-geostrophic ocean dynamics in eddy-resolving regimes, *Ocean Modelling*, **94** (2015), 1-14.
[29] L. Thiry, L. Li, G. Roullet and E. Mémin, Mqgeometry-1.0: A multi-layer quasi-geostrophic solver on non-rectangular geometries, *Geoscientific Model Development*, **17** (2024), 1749-1764.
[30] G. K. Vallis, *Atmospheric and Oceanic Fluid Dynamics*, Cambridge University Press, 2017.
[31] G. K. Vallis, *Essentials of Atmospheric and Oceanic Dynamics*, Cambridge University Press, 2019.
[32] W. T. Verkley, A balanced approximation of the one-layer shallow-water equations on a sphere, *Journal of the Atmospheric Sciences*, **66** (2009), 1735-1748.
[33] J. Wallace and P. Hobbs, *Atmospheric Science: An Introductory Survey*, Elsevier, 2006.
[34] L. Wang, S. Hardiman, P. Bett, R. Comer, C. Kent and A. Scaife, What chance of a sudden stratospheric warming in the southern hemisphere?, *Environmental Research Letters*, **15** (2020), 104038.
[35] D. S. Watkins, Isospectral flows, *SIAM Review*, **26** (1984), 379-391.
[36] Z. Xiao, M. Wan, S. Chen and G. L. Eyink, Physical mechanism of the inverse energy cascade of two-dimensional turbulence: A numerical investigation, *Journal of Fluid Mechanics*, **619** (2009), 1-44.
[37] V. Zeitlin, Finite-mode analogs of 2D ideal hydrodynamics: Coadjoint orbits and local canonical structure, *Physica D: Nonlinear Phenomena*, **49** (1991), 353-362.
[38] V. Zeitlin, Self-consistent finite-mode approximations for the hydrodynamics of an incompressible fluid on nonrotating and rotating spheres, *Physical Review Letters*, **93** (2004), 264501.

Received August 25, 2025; revised January 16, 2026.